separations

Article

Adsorption of Fluoride from Water Using Aluminum-Coated Silica Adsorbents: Comparison of Silica Sand and Microcrystalline Silica

Kiana Modaresahmadi, Amid P. Khodadoust * and James Wescott

Department of Civil, Materials, and Environmental Engineering, University of Illinois Chicago, Chicago, IL 60607, USA; kmodar2@uic.edu (K.M.); jwesco3@uic.edu (J.W.)
* Correspondence: akhodado@uic.edu

Abstract: Two aluminum-coated silica adsorbents were evaluated using silica sand and microcrystalline silica as aluminum-oxide-based adsorbents with different crystalline silica base materials. The aluminum coating contained mainly amorphous aluminum oxides for both aluminum-coated silica adsorbents. The adsorption of fluoride onto both adsorbents was favorable according to the Langmuir and Freundlich adsorption equations, while the physical adsorption of fluoride occurred for both adsorbents according to the Dubinin–Raduskevish (D-R) equation. The adsorption of fluoride was stronger for aluminum-coated silica sand based on adsorption parameters from the Langmuir, Freundlich, and D-R adsorption equations, with the stronger binding of fluoride likely due to the observed greater specific adsorption. The adsorption capacity determined using the Langmuir equation was about 7 times greater for aluminum-coated microcrystalline silica primarily due to the 1.22-orders-of-magnitude-larger surface area of aluminum-coated microcrystalline silica, whereas the surface-normalized adsorption capacity was 2.4 times greater for aluminum-coated silica sand, possibly due to more aluminum being present on the surface of silica sand. Fluoride adsorption occurred over a broad pH range from 3 to 10 for both adsorbents, with nearly the same pH_{PZC} of 9.6, while aluminum-coated microcrystalline silica displayed a higher selectivity for fluoride adsorption from different natural water sources.

Keywords: adsorption; aluminum; coating; fluoride; microcrystalline silica; silica sand

Citation: Modaresahmadi, K.; Khodadoust, A.P.; Wescott, J. Adsorption of Fluoride from Water Using Aluminum-Coated Silica Adsorbents: Comparison of Silica Sand and Microcrystalline Silica. *Separations* **2024**, *11*, 125. https://doi.org/10.3390/separations11040125

Academic Editor: Alena Kubatova

Received: 19 March 2024
Revised: 15 April 2024
Accepted: 16 April 2024
Published: 19 April 2024

1. Introduction

Although water fluoride concentrations of less than 1 mg/L are beneficial to the human body as fluoride helps to prevent tooth decay, higher concentrations of fluoride in water can lower calcium levels in the body and cause problems such as fluoroscopic, brittle bones, and brain damage [1]. The fluoride in water is mostly derived through the slow breakdown of fluoride minerals such as fluorite (CaF_2) in groundwater, while anthropogenic sources of fluoride like mining, industrial waste such as battery manufacturing or semiconductor production, and the use of phosphate fertilizers in farms can increase water fluoride pollution levels to 1000 mg/L. Fluoride has been found in surface water such as lakes and rivers, and, while fluoride concentration was within the safety limits in most rivers, this quantity reached 2800 mg/L in geothermal springs [2,3]. The fluoride levels in groundwater from the US western and southern states have been found to be elevated, with concentrations reaching 15.9 mg/L in Idaho, 7.4 mg/L in Arizona, 13.0 mg/L in New Mexico, 12.0 mg/L in Oklahoma, 11.2 mg/L in Colorado, and 8.8 mg/L in Texas [4]. About 2.5 billion people worldwide rely on groundwater, and this demand is expected to increase by 30% by 2050 [5,6]. The World Health Organization (WHO) established an international safe fluoride daily limit of 1.5 mg/L in drinking water to protect human health [7].

The removal of fluoride from water may be carried out using several technologies, including chemical precipitation [8], reverse osmosis/nano-filtration [9,10], ion exchange [11], electrodialysis [12], electrocoagulation [13], adsorption [14], or a combination of the aforementioned technologies which have been investigated and developed [15]. Each technology has advantages and disadvantages that must be considered, such as reverse osmosis, which has a high fluoride removal percentage but can also remove essential ions from water, necessitating another step of mineralization and making the overall process more expensive than the other methods [16]. Precipitation is often only appropriate for water with a high degree of fluoride contamination, i.e., greater than 100 mg/L, and cannot be employed at lower fluoride concentrations [17]. The efficiency of fluoride removal using ion exchange technology is highly dependent on the nature of the water being treated, such as the level of alkalinity or the presence of cations or anions, in addition to the high waste and disposal costs associated with the regeneration or recharging of spent ion exchange media [18].

Among all of these methods, adsorption technology offers advantages for the removal of fluoride because of its simplicity of application and low maintenance in the short and long term, as well as its cost-effectiveness due to the ability to use different materials as sorbents that are suitable, compatible, and cheap in the region that is using this method [19] and the capability of recycling and reusing used sorbents for several cycles, later being able to be used as byproducts in different contexts. Moreover, the adsorption technique is capable of treating the target pollutant at both high and low concentrations [20]. In the adsorption technique, natural or synthetic adsorbents must be designed from a variety of materials such as high-valency metals, functionalized sorbents such as carbon-based materials, industrial waste, bio-sorbents, and others, such that the adsorbent's surface can retain the target contaminant via physical or chemical processes [21]. Metal oxides, particularly activated alumina- and other aluminum-based sorbents [17,20,22], are among the most commonly used sorbents for the removal of fluoride and other pollutants from water, including heavy metals and inorganic contaminants. However, there are some drawbacks to alumina- and aluminum-based sorbents' application, such as the use of caustic chemicals during the regeneration process, which causes fouling of the filter bed media, a relatively slow rate of adsorption, and a suboptimal fluoride removal performance under neutral-to-alkaline pH conditions [23–27]. Numerous efforts have been undertaken to improve the effectiveness of alumina- and aluminum-based sorbents. Among these initiatives are the development of aluminum composites with a mixture of other metal oxides, either as binary or ternary sorbents, and the application of aluminum as a coating on different substrate materials [28–33].

In this study, two aluminum based adsorbents were developed by applying aluminum as a single metal coating for two crystalline silica support materials with different particle sizes: silica sand (larger particle size) and microcrystalline silica (smaller particle size). A comparison of the two crystalline silica aluminum-coated adsorbents assessed the fluoride adsorption performance of two aluminum-coated adsorbents with a similar sorbent base support material but with different particle sizes. The availability and suitability of sand for its application as a filtration medium in continuous flow systems, as well as its ability to remove bacteria and suspended particulates along with its non-toxic nature, make it a good choice for water treatment applications. Microcrystalline silica may be used alone in batch adsorption systems or may be mixed in with an inert solid material of a larger grain size to provide greater hydraulic conductivity in packed beds for flow-through adsorption systems. The two aluminum-coated silica base adsorbents developed in this study, aluminum-coated silica sand (AlCSS) and aluminum-coated microcrystalline silica (AlCMS), were evaluated for their adsorption and removal of fluoride as a function of time, adsorbent dosage, solution pH, and the presence of co-existing ions.

2. Materials and Methods

2.1. Materials

Microcrystalline silicon (IV) oxide (99.5% purity) with a particle size of less than 10 microns (μm) was supplied by Thermo-Fisher Scientific (Fairlawn, NJ, USA). Quartz silica sand with an average particle size of 250 microns (50–70 US mesh) was provided by Sigma-

Aldrich (St. Louis, MO, USA). Aluminum chloride hexahydrate (99% purity, ACS grade), hydrochloric acid (ACS plus grade), sodium hydroxide (ACS reagent pellets), sodium fluoride (ACS grade), sodium bicarbonate (ACS grade), sodium sulfate (ACS grade), and calcium chloride dihydrate (99% purity, ACS grade) were all provided by Fisher Scientific (NJ, USA). All the solutions were prepared using de-ionized (DI) water that had a resistivity greater than 18 MΩ, available in the laboratory. A 1000 mg/L fluoride stock solution was obtained by dissolving 2.21 g NaF in 1 L DI water; the fluoride stock solution was diluted using DI water to prepare various solutions with different fluoride concentrations.

2.2. Preparation of AlCSS and AlCMS Sorbents

For the preparation of aluminum-coated microcrystalline silica (AlCMS), 40 g of microcrystalline silica was weighed on a scale before being mixed with 100 mL of a 1 M aluminum chloride coating solution. This mixture was left to stir for 24 h on a mixing table. The coating solution was centrifuged for 10 min to separate it from the microcrystalline silica. Following this, the sorbent was dried in an oven at 110 °C for 24 h before being calcined in a furnace for 24 h at 220 °C. For the preparation of the aluminum-coated silica sand (AlCSS), 40 g of silica sand was mixed with 100 mL of a 1 M aluminum chloride solution on a mixing table for 24 h. The coating solution was subsequently decanted from the silica sand. The wet-coated silica sand was then transferred to an oven and dried for 24 h at 110 °C before being calcined in a furnace for 24 h at 220 °C. The prepared AlCMS and AlCSS sorbents were allowed to cool down to room temperature before being stored in high-density polyethylene (HDPE) bottles.

2.3. Characterization of the AlCSS and AlCMS Sorbents

The mineral phases of the AlCSS and AlCMS sorbents were studied using X-ray powder diffraction (XRD) to determine if the coating was amorphous or crystalline. The XRD analysis was performed using the XRD-Bruker D8 Discover System (Billerica, MA, USA) from 2θ = 10° to 80° at 40 KV and 30 mA with a Cu tube (1.5418 Å). The specific surface area of the AlCSS and AlCMS sorbents was investigated using the Brunauer–Emmett–Teller (BET) method using an accelerated surface area and porosimeter system (Micromeritics Instrument Corporation, Norcross, GA, USA). Scanning electron microscopy (SEM) and SEM with electron-dispersive X-ray spectroscopy (EDX) were performed to examine the surface morphology and elemental composition of the AlCSS and AlCMS sorbent surfaces using a TOPCON ABT-150S SEM with a EDX instrument (Tokyo, Japan). Transmission electron microscopy (TEM) was used to investigate the microstructure of the AlCSS and AlCMS sorbents, employing a JEOL JEM-3010 300 kV TEM instrument (Tokyo, Japan).

2.4. Batch Adsorption Experiments

Batch adsorption experiments were carried out to assess the equilibrium, kinetic behavior, and effect of the pH and co-existing ions on the performance of the AlCSS and AlCMS sorbents for the removal of fluoride. For each batch adsorption experiment, 1 g of sorbent was mixed with 50 mL of a 5 mg/L fluoride solution in a 50 mL polypropylene bottle, and the bottle was then placed in a rotating tumbler at 20 rpm. After 24 h of mixing, the sample was centrifuged at 9000 rpm for 10 min, and 10 mL of the centrifuged solution was separated. The concentration of fluoride in the solution was measured with a Thermo Scientific Orion (Waltham, MA, USA) fluoride ion-selective electrode according to Standard Method 4500 F^- [34]. All the batch adsorption experiments were performed in triplicate. The fluoride removal efficiency and adsorption capacity of the AlCSS and AlCMS sorbents were determined as follows:

$$\text{Removal}(\%) = (C_0 - C_e)/C_0 \times 100\% \tag{1}$$

$$q_e = (C_0 - C_e)/m \times V \tag{2}$$

The fluoride adsorption (capacity) is q_e (mg/kg) at equilibrium, with the initial and final fluoride concentrations represented by C_0 and C_e, respectively. In this equation, the mass of the AlCSS and AlCMS sorbents is represented as m (kg), while the volume of the fluoride solution is denoted as V (L).

2.5. Adsorption Isotherm Models

The Langmuir, the Freundlich, and the Dubinin–Radushkevich (D-R) adsorption equilibrium isotherm models were used to determine the adsorption parameters for describing the adsorption of fluoride onto the AlCSS and AlCMS sorbents. The linearized form of the Langmuir adsorption equation [35] and the corresponding factor for adsorption favorability (R_L) are shown as follows:

$$C_e/q_e = C_e/q_m + 1/K_L q_m \tag{3}$$

$$R_L = 1/(1 + K_L C_0) \tag{4}$$

where q_m (mg/kg) and q_e (mg/kg) represent the adsorbent's maximum and equilibrium adsorption capacities, respectively. The C_0 and C_e are the initial concentration and equilibrium concentration of the adsorbate in the solution, respectively. The Langmuir adsorption parameter K_L denotes the adsorption strength (L/mg) of the adsorbent. An R_L value between zero and one indicates the favorability of the adsorption process. The linearized form of the Freundlich adsorption equation [36] is shown as follows:

$$log q_e = log K_F + 1/n \log C_e \tag{5}$$

where K_F is related to the adsorption capacity, and *1/n* is related to the adsorption strength of the adsorbent. The favorability of the adsorption process is indicated by a $1/n$ value less than one. The linearized form of the Dubinin–Radushkevich (D-R) adsorption equation [37] and the value of the Polanyi potential (ε) in the D-R equation are shown as follows:

$$\ln q_e = \ln q_m - K_{D-R}\, \varepsilon^2 \tag{6}$$

$$\varepsilon = \mathrm{RT} \ln (1 + 1/C_e) \tag{7}$$

The $K_{D\text{-}R}$ is the Dubinin–Radushkevich (D-R) constant, T is the absolute temperature (degrees *K*), and R is the universal gas constant (8.314 J/mol K). The mean free energy (*E*) determined from the Dubinin–Radushkevich (D-R) constant $K_{D\text{-}R}$ distinguishes between physical adsorption ($E < 8$ kJ/mol) and chemical adsorption (8 kJ/mol $< E <$ 16 kJ/mol), where

$$E = 1/\sqrt{(2K_{D-R})} \tag{8}$$

2.6. Effect of pH on Fluoride Removal

The effect of pH on fluoride removal using the AlCSS and AlCMS sorbents was studied using batch adsorption experiments. This investigation involved adjusting the initial solution pH from 3 to 11 using 0.1 M NaOH and 0.1 M NaCl solutions. The fluoride removal percentage and the final pH values were determined. All the pH experiments were performed in triplicate.

2.7. Effect of Co-Existing Ions and Effect of Water Types on Fluoride Removal

The effect of common co-existing ions on the removal of fluoride was investigated. Solutions of co-existing ions were prepared individually for calcium (Ca^{2+}), bicarbonate (HCO_3^-), and sulfate (SO_4^{2-}), where ion concentrations of 0.5 mM, 1 mM, 2 mM, and 5 mM of each ion were selected. All the ion solutions were spiked with an initial fluoride concentration of 5 mg/L. The combined influence of these co-existing ions in synthetic water was also investigated, with 1 mM (40 mg/L) of calcium, 2.5 mM (152 mg/L) of bicarbonate, and 1 mM (96 mg/L) of sulfate spiked with an initial fluoride concentration of 5 mg/L. The removal of fluoride was also evaluated for several types of natural water sources, each spiked with 5 mg/L of fluoride: groundwater type 1, groundwater type 2, and Chicago municipal tap water sourced from a fresh-water lake. The effect of co-existing ions and different water types was studied using batch adsorption experiments in triplicate. Table 1 provides information on the water quality parameters, including pH, TDS (total dissolved solids), alkalinity, total hardness (TH), and the initial fluoride levels present before any fluoride spiking, across different water types.

Table 1. Quality criteria of various water types.

Water Types	pH	TDS (mg/L)	Alkalinity (mg/L as $CaCO_3$)	Total Hardness (mg/L as $CaCO_3$)	Background Fluoride Concentration (mg/L)
Synthetic water	7.99	340	125	100	0
Tap water	7.86	171	103	140	0.9
Groundwater (type 1)	8.47	303	202	273	0.7
Groundwater (type 2)	7.91	1220	150	796	0.3

2.8. Zeta Potential Experiments

The point of zero charge (PZC) was determined by employing 0.5 g of each of the AlCSS and AlCMS sorbents in 1000 mL of a 1 mM NaCl solution without any fluoride in the solution and with 5 mg/L fluoride in the solution using the Zeta-meter system 3.0 (Zeta meter Inc., Staunton, VA, USA). The initial pH of the solution was varied for a pH range of 5 to 11, using 0.1 M HCl and 0.1 M NaOH solutions; the experiments were performed in triplicate.

2.9. Successive Adsorption Cycles' Study

To evaluate the fluoride removal performance of the AlCSS and the AlCMS sorbents in several successive adsorption cycles, the removal of fluoride was determined for the two sorbents using five consecutive batch adsorption cycles. For each sorbent, one gram of the sorbent was mixed with 50 mL of a 5 mg/L fluoride solution for 24 h using the batch adsorption experiment procedure. After 24 h of mixing, the spent solution was separated from the spent sorbent by centrifugation for 10 min at 9000 rpm; the spent sorbent was then mixed with 50 mL of fresh 5 mg/L fluoride solution for the next 24 h adsorption cycle. These batch adsorption experiments were carried out in triplicate for five consecutive 24 h adsorption cycles.

3. Results and Discussion

3.1. Characterization of the AlCSS and AlCMS Sorbents

The surface morphology of the AlCSS and AlCMS sorbents is depicted in the SEM micrographs in Figure 1. As shown in Figure 1a, the AlCSS sorbent particle size was in the range of 250 microns, while the aluminum coating occurred in clusters on the silica sand surface with cluster sizes of about 10–25 microns. As shown in Figure 1b, the AlCMS sorbent particles were in the size range of 2–10 microns, with the aluminum coating dispersed on the sorbent surface. The SEM-EDX results for the AlCSS and AlCMS sorbents are shown in Figure 2. The SEM-EDX results indicate the presence of aluminum on the surface of both the AlCSS and AlCMS sorbents in addition to silicon and oxygen; the results also show that more aluminum was present on the surface of the AlCSS sorbent (Figure 2a) than on the surface of the AlCMS sorbent (Figure 2b). The BET surface area of the AlCSS sorbent and AlCMS sorbent was determined to be 0.6285 m^2/g and 10.5021 m^2/g, respectively.

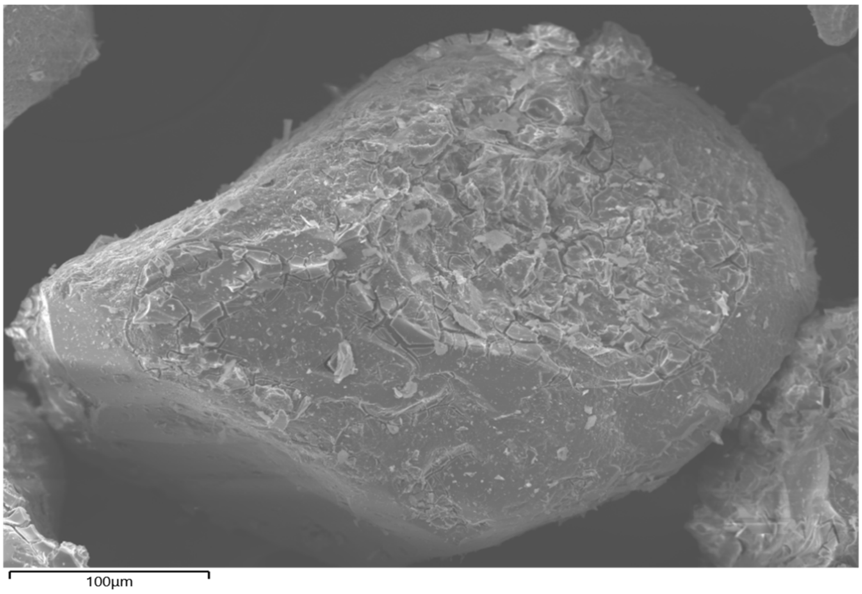

(**a**)

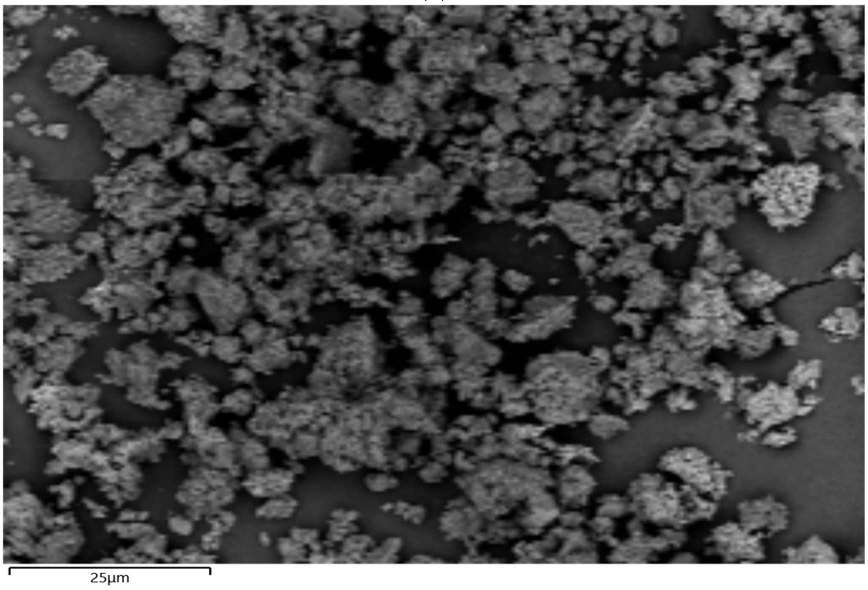

(**b**)

Figure 1. SEM micrographs: (**a**) AlCSS sorbent and (**b**) AlCMS sorbent.

Figure 3 depicts the XRD patterns of the AlCSS and AlCMS sorbents. The results from Figure 3 indicate that the aluminum coating for both adsorbents was amorphous because no crystalline peaks relating to aluminum (oxides) were observed for the AlCSS and AlCMS sorbents, while crystalline silica (SiO_2) peaks were detected for both the AlCSS and AlCMS sorbents due to the silica sand and the microcrystalline silica supporting materials. Furthermore, the XRD pattern results for both silica sand and microcrystalline silica before coating (Figure S1a,b) show the same XRD peaks, with a higher intensity, as the AlCSS and AlCMS sorbents (Figure 3), confirming the presence of crystalline silica (SiO_2) on the surface of the AlCSS and AlCMS sorbents. The TEM micrographs presented in Figure 4 show that the aluminum coatings of both the AlCSS (A,B) and AlCMS (C,D) sorbents were mostly amorphous, with little crystallinity, in contrast to the highly crystalline base materials of the AlCSS sorbent (silica sand) and the AlCMS sorbent (microcrystalline silica).

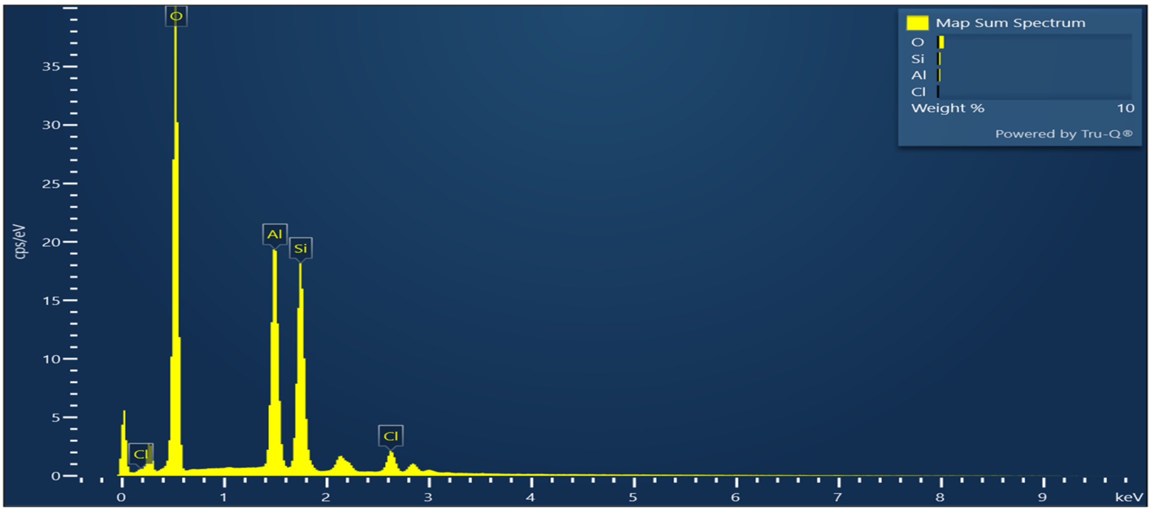

(**a**)

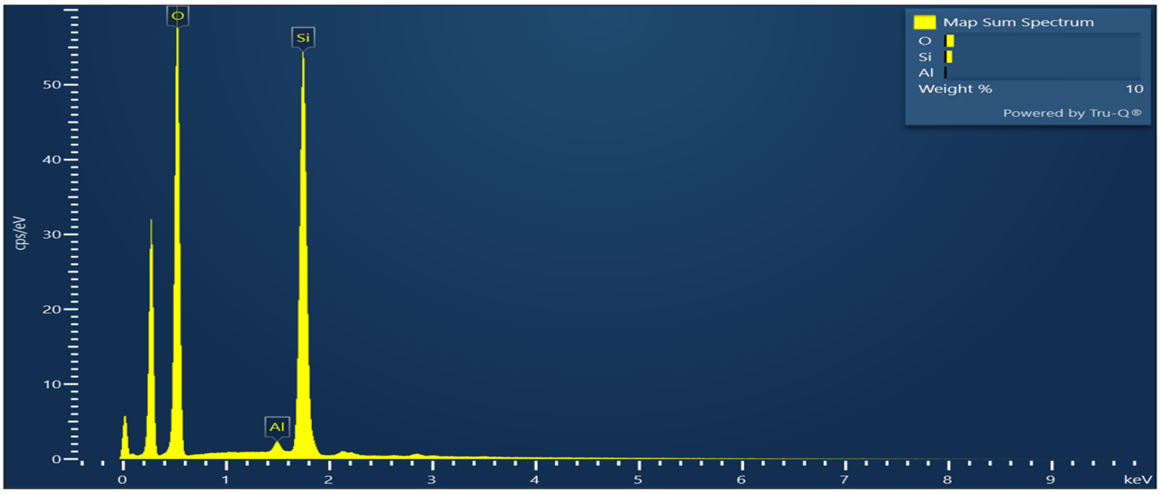

(**b**)

Figure 2. SEM-EDX Spectra for (**a**) AlCSS sorbent and (**b**) AlCMS sorbent.

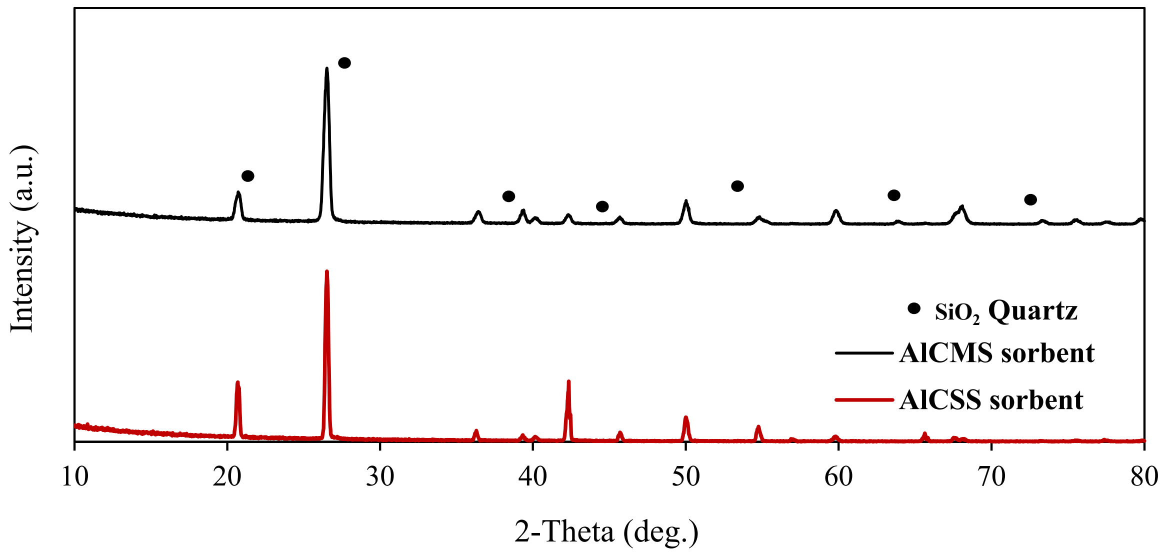

Figure 3. XRD patterns of the AlCSS and AlCMS sorbents.

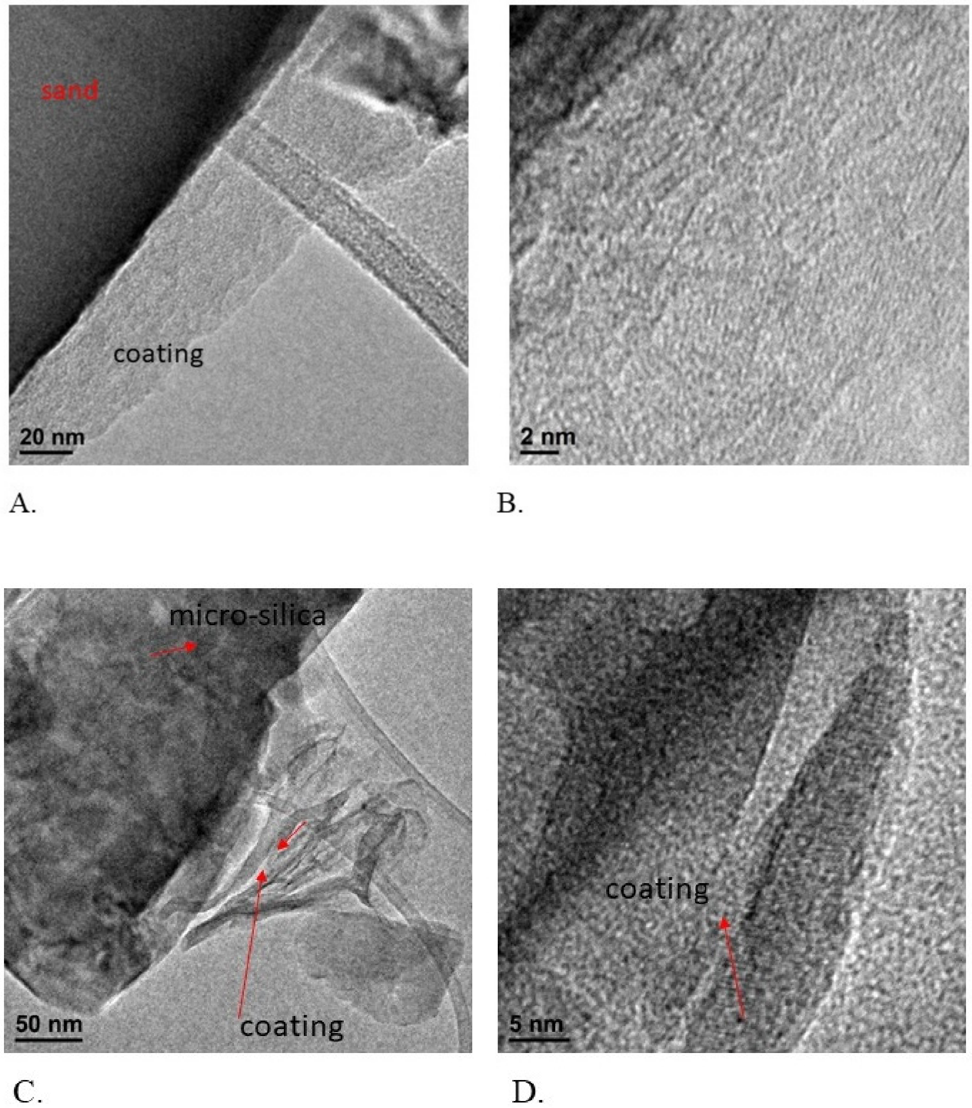

Figure 4. TEM micrographs of the AlCSS sorbent (**A**,**B**) and the AlCMS sorbent (**C**,**D**).

Although the non-uniform distribution of aluminum coating was observed, there was a marked difference in the level of aluminum on the surface of the two sorbents, where higher levels of aluminum were present on silica sand than on microcrystalline silica. The weight percentages of aluminum present on the crystalline silica surfaces obtained from the SEM/EDX results were as follows: average of 19.4% (15.8% to 24.6%) for the AlCSS sorbent; and average of 3% (1.3% to 5.4%) for the AlCMS sorbent.

3.2. Adsorption Kinetics

The removal of fluoride from water by the AlCSS and AlCMS sorbents as a function of contact time is shown in Figure 5. Both the AlCSS and AlCMS sorbents removed more than 70 percent of fluoride rapidly in 30 min. Fluoride removal increased to around 90% after six hours and became greater than 90% after 24 h for the AlCMS sorbent, while fluoride removal increased to around 85% after six hours and became greater than 90% after 24 h for the AlCSS sorbent. Fluoride adsorption reached equilibrium after 12 and 24 h, with experimental equilibrium adsorption capacities of 240.9 mg/kg and 242.8 mg/kg for the AlCMS and AlCSS sorbents, respectively. While the removal of fluoride using the AlCSS and the AlCMS sorbents was greater than 90%, the removal of fluoride using an adsorbent dosage of 20 g/L for both uncoated crystalline silica base materials was determined to be about 1.9% and 10%, for uncoated silica sand and uncoated microcrystalline silica, respectively.

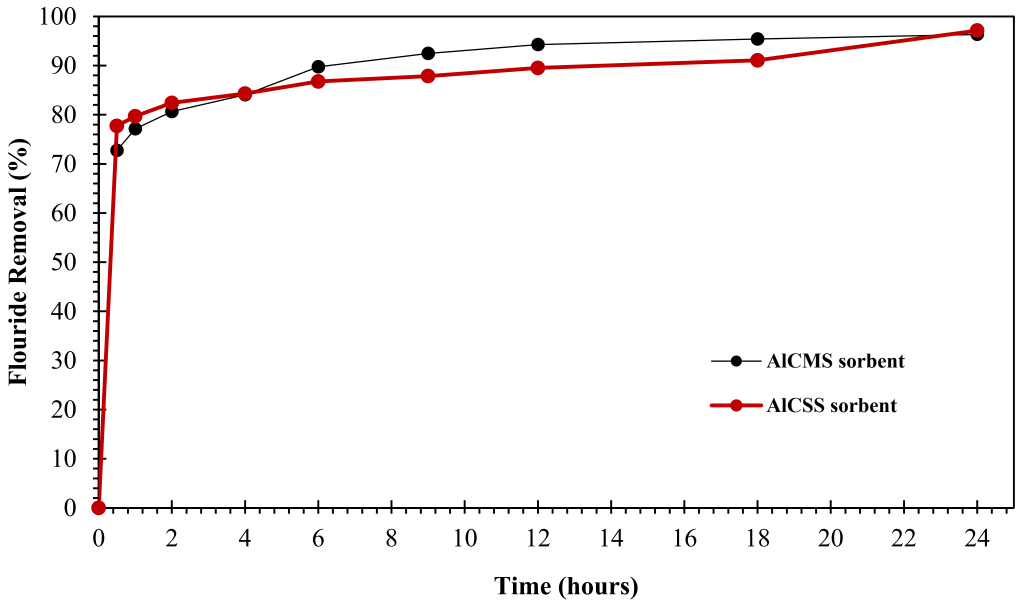

Figure 5. Adsorption of fluoride by the AlCSS and AlCMS sorbents as a function of time using an initial fluoride concentration of 5 mg/L and an adsorbent dosage of 20 g/L.

The fluoride adsorption kinetics of the AlCSS and AlCMS sorbents were investigated using the pseudo-first-order kinetics model [38] and the pseudo-second-order kinetics model [39]. The linear forms of the pseudo-first-order model and the pseudo-second-order model used to fit the adsorption kinetics data are shown in Equations (9) and (10), respectively, as follows:

$$ln(q_e - q_t) = lnq_e - k_1 t \quad (9)$$

$$t/q_t = 1/k_2 q_e^2 + t/q_e \quad (10)$$

The fluoride uptake per unit mass of adsorbent at equilibrium and time t is represented by q_e (mg/kg) and q_t (mg/kg), respectively. The k_1 (1/min) and k_2 (g/mg. min) values also reflect the first-order and second-order adsorption rate constants, respectively. The values of k_1 were derived from the slope of a linear plot of ln ($q_e - q_t$) against time, as shown in Figure S2a. Similarly, the calculation of k_2 was based on the slope of a linear plot of t/q_t versus time, as shown in Figure S2b. The adsorption kinetics parameters determined using the pseudo-first-order and pseudo-second-order kinetics models for both the AlCSS and AlCMS sorbents are shown in Table 2. The results show that the AlCMS and AlCSS sorbents both followed pseudo-second-order kinetics, with R^2 values of 0.9997 and 0.9975, respectively, while the calculated q_e values for the AlCMS and AlCSS sorbents were 243.9 mg/kg and 238.1 mg/kg, respectively; the calculated q_e values closely matched their experimental q_e values of 240.9 mg/kg and 242.8 mg/kg, respectively, where q_e was the amount of fluoride adsorbed after 24 h. The adsorption kinetics followed the pseudo-second-order kinetics model for both sorbents, indicating that there was more than one rate-limiting process affecting the adsorption of fluoride onto both sorbents. The results from Table 2 show the pseudo-second-order rate constant k_2 values of 0.1688 (g/mg. min) and 0.1480 (g/mg. min) for the AlCMS sorbent and the AlCSS sorbent, respectively.

The Weber and Morris equation [40] was employed to evaluate intraparticle diffusion as follows:

$$q_t = \mathrm{k}_{id}\mathrm{t}^{\frac{1}{2}} + C \quad (11)$$

The intraparticle diffusion rate constant and the boundary layer effect are represented by k_{id} and C, respectively. Based on the results presented in Table 2, the intercept C had non-zero values for both the AlCSS and AlCMS sorbents, indicating that intraparticle diffusion was not the only rate-controlling process affecting the adsorption of fluoride for both sorbents. The adsorption kinetics data were plotted based on Equation (11) in Figure

S3; the plots from Figure S3a,b show that the second segment of the plots for the AlCSS and AlCMS sorbents had appreciable slopes (for $t^{1/2}$ from 5 to 38), while the first segment of the plots had very steep slopes (for $t^{1/2}$ from 0 to 5). While the steep slopes of the first segment of the plots indicate that external mass transfer influenced the adsorption process, the less-steep slopes of the second segment of the plots indicate that intraparticle diffusion also influenced the adsorption process. The results shown in Figure S3, therefore, indicate that the adsorption of fluoride onto the AlCSS sorbent (Figure S3a) and the AlCMS sorbent (Figure S3b) was influenced by both external mass transfer and intraparticle diffusion. The second segment of the plot had a steeper slope for the AlCMS sorbent (Figure S3b) than for the AlCSS sorbent (Figure S3a), indicating that intraparticle diffusion influenced the adsorption of fluoride for the AlCMS sorbent to a greater extent than for the AlCSS sorbent, likely due to the smaller particle size and larger surface area of the AlCMS sorbent.

Table 2. Adsorption kinetics parameters for fluoride adsorption onto the AlCSS and AlCMS sorbents.

		AlCSS Sorbent	AlCMS Sorbent
	Experimental q_e (mg/kg)	242.8	240.9
Pseudo-first-order kinetics model	k_1 (1/min)	0.0033	0.0027
	q_e (mg/kg)	95.6	71.6
	R^2	0.7363	0.8791
Pseudo-second-order kinetics model	k_2 (g/mg-min)	0.1480	0.1688
	q_e (mg/kg)	238.1	243.9
	R^2	0.9975	0.9997
Intraparticle diffusion kinetics model	k_{id} (mg/g-min$^{1/2}$)	3.806	4.208
	C	125.80	120.16
	R^2	0.4533	0.5229

The results from the XRD analysis (Figure 3) and TEM analysis (Figure 4) showed that the aluminum coating was amorphous for both the AlCSS and AlCMS sorbents. Some intraparticle diffusion of fluoride in the aluminum coating possibly occurred due to the amorphous nature of the aluminum coating on the crystalline silica surface. The results obtained for the adsorption of fluoride using uncoated silica sand and uncoated microcrystalline silica showed that small amounts of fluoride were adsorbed onto the crystalline silica base materials, so it was possible that small amounts of fluoride adsorbed onto the silica base materials of the aluminum-coated silica sorbents, but the majority of fluoride adsorption occurred onto the aluminum coating present on the silica base materials.

3.3. Adsorption Equilibrium

The effect of adsorbent dosage on the removal of fluoride was evaluated using a fluoride solution with an initial fluoride concentration of 5 mg/L. Figure 6 shows the effect of adsorbent dosage on the removal of fluoride using the AlCSS and AlCMS sorbents. The results show that the removal of fluoride was not affected significantly by sorbent dosage for the AlCMS sorbent, from a 2 g/L to 8 g/L sorbent dosage, while the removal of fluoride increased appreciably from 42% to 92% for the AlCSS sorbent, from a 2 g/L to 8 g/L sorbent dosage, respectively. The removal of fluoride was similar for both the AlCSS and AlCMS sorbents at sorbent dosages of 8 g/L and higher. At sorbent dosages less than 8 g/L, the sorbent with the larger surface area removed more fluoride, but there was no significant effect of sorbent surface area observed at sorbent dosages of 8 g/L and higher. As a result, the 2 g/L dosage of the AlCMS sorbent and the 8 g/L dosage of the AlCSS sorbent were selected to carry out adsorption equilibrium isotherm experiments for the two adsorbents.

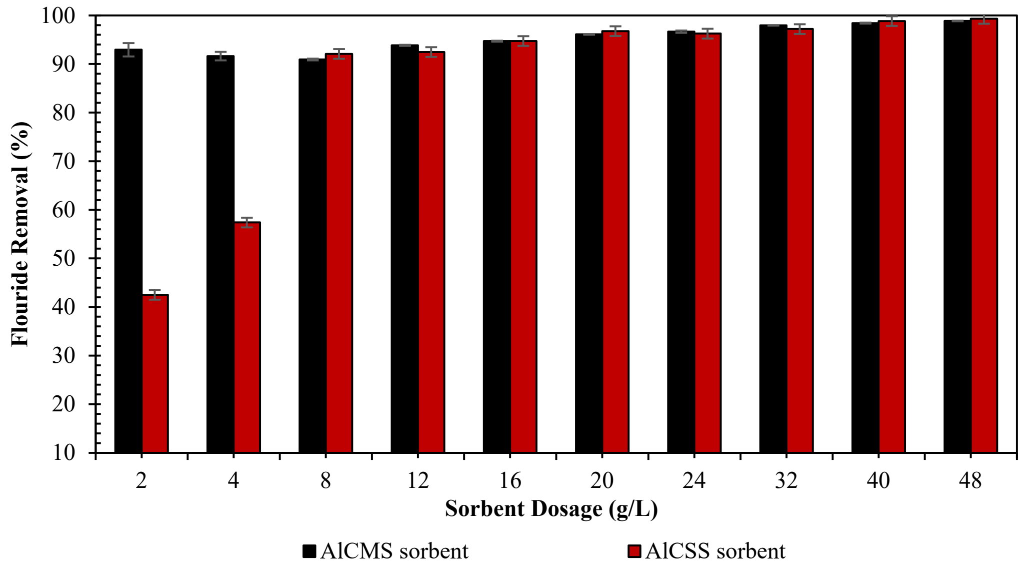

Figure 6. Effect of adsorbent dosage by the AlCSS and AlCMS sorbents on the removal of fluoride using a 5 mg/L initial fluoride solution for 24 h.

Figure 7 shows the effect of the initial fluoride concentration on the removal of fluoride using a dosage of 8 g/L for both the AlCSS sorbent and the AlCMS sorbent. The results show that the removal of fluoride using the AlCMS sorbent was not significantly affected for an initial fluoride concentration ranging from 3 to 15 mg/L, while fluoride removal decreased gradually with increasing initial fluoride concentrations higher that 15 mg/L, whereas fluoride removal using the AlCSS sorbent decreased with increasing initial fluoride concentrations higher than 5 mg/L. The results show that higher initial concentrations of fluoride affected the removal of fluoride to a greater extent for the AlCSS sorbent than the AlCMS sorbent, mainly due to the larger surface area of the AlCMS sorbent providing a higher number of active adsorption sites available for adsorption of fluoride.

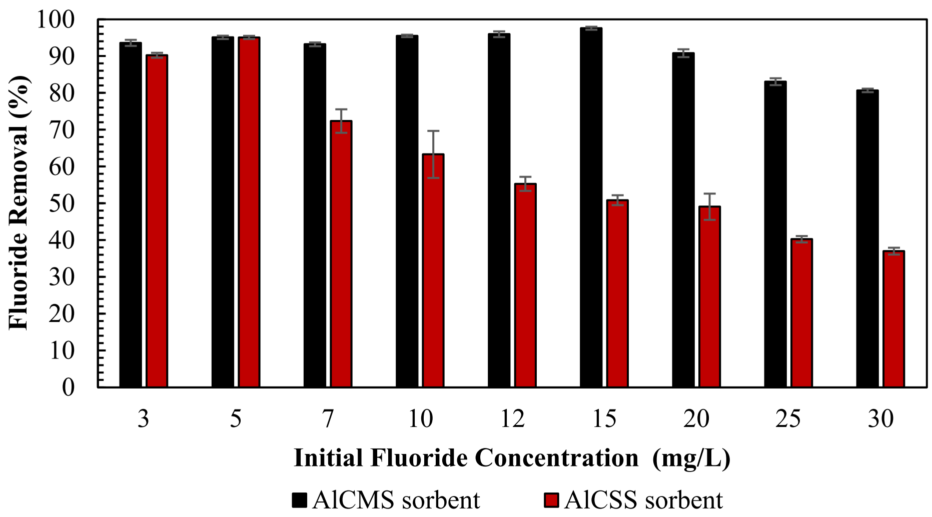

Figure 7. Effect of initial fluoride concentration on the removal of fluoride using an 8 g/L adsorbent dosage for both the AlCSS and AlCMS sorbents for 24 h.

The adsorption equilibrium isotherm data for the adsorption of fluoride onto the AlCSS and AlCMS sorbents are presented in Figure 8.

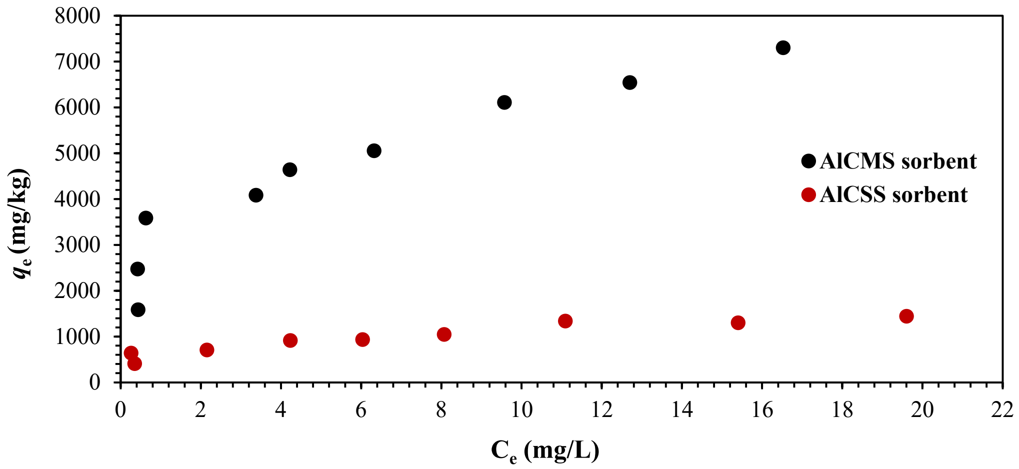

Figure 8. Adsorption equilibrium isotherm data for the adsorption of fluoride onto 2 g/L of AlCMS sorbent and 8 g/L of AlCSS sorbent over 24 h with an initial fluoride concentration of 3 to 30 mg/L.

The adsorption equilibrium parameters for both the AlCMS and the AlCSS sorbents determined using the three linearized adsorption equilibrium equations are presented in Table 3. The adsorption equilibrium isotherm data presented in Figure 8 follow the linearized form of the Langmuir adsorption equation, with R^2 values of 0.969 and 0.972 for the AlCSS and AlCMS sorbents, respectively. The results in Table 3 show that the maximum adsorption capacities determined from the Langmuir adsorption equation were 10,000 mg/kg and 1430 mg/kg for the AlCMS and AlCSS sorbents, respectively. The adsorption capacity of the AlCMS sorbent was nearly seven times greater than the adsorption capacity of the AlCCS sorbent, mainly due to the larger surface area of the AlCMS sorbent. The Langmuir adsorption capacities obtained for the AlCSS and AlCMS sorbents were similar to the Langmuir adsorption capacities reported for several activated alumina adsorbents, such as 1450 mg/kg [27], 4040 mg/kg [41], and 1077 mg/kg [42], and 7870 mg/kg for aluminum-oxide-coated pumice [26]; these reported adsorption capacities were mostly in the range of values obtained for the AlCSS and AlCMS sorbents (1430–10,000 mg/kg). The K_L values for the AlCSS sorbent and the AlCMS sorbent were 0.5 L/mg and 0.333 L/mg, respectively; the K_L values obtained for the AlCSS and AlCMS sorbents were comparable to the K_L values reported for several alumina-based adsorbents: 0.31 L/mg [27], 0.675 L/mg [41], 0.177 L/mg [42], and 0.087 L/mg [26].

Table 3. Adsorption equilibrium parameters for the adsorption of fluoride onto the AlCSS and AlCMS sorbents.

Adsorbent	Langmuir	Freundlich	Dubinin–Radushkevich
AlCSSsorbent	q_{mL} = 1430 mg/kg K_L = 0.50 L/mg R^2 = 0.9694	1/n = 0.2432 K_F = 657 mg/kg R^2 = 0.8652	K_{DR} = 5.39 × 10^{-8} E = 3.05 kJ/mol R^2 = 0.5738
AlCMSsorbent	q_{mL} = 10,000 mg/kg K_L = 0.333 L/mg R^2 = 0.9727	1/n = 0.3153 K_F = 2948 mg/kg R^2 = 0.8663	K_{DR} =1.143 × 10^{-7} E = 2.09 kJ/mol R^2 = 0.8171

The results from Table 3 show that the adsorption equilibrium isotherm data follow the linearized Freundlich equation, with R^2 values of 0.865 and 0.866 for the AlCSS and AlCMS sorbents, respectively. The Freundlich adsorption constants K_F and $1/n$ were determined to be 2948 mg/kg and 0.3153 for the AlCMS sorbent and 657 mg/kg and 0.243 for the AlCSS sorbent, respectively. The favorable adsorption of fluoride occurred for both the AlCMS and the AlCSS sorbents, based on R_L values between 0 and 1 for the AlCMS sorbent (0.6) and the AlCSS sorbent (0.286) and *1/n* values of less than one for the AlCMS sorbent (0.3153) and the AlCSS sorbent (0.2432). The mean free energy E was determined to be 2.09 kJ/mol for the AlCMS sorbent and 3.05 kJ/mol for the AlCSS sorbent, suggesting that the adsorption of fluoride onto both the AlCSS and AlCMS sorbents was mainly physical adsorption.

The best fit of data (highest R^2 values greater than 0.95) was obtained for the Langmuir adsorption model for both the AlCSS and the AlCMS sorbents, indicating that the adsorption of fluoride onto the surfaces of both the AlCSS and the AlCMS sorbents occurred mostly as monolayer adsorption for adsorption sites with similar adsorption energies, while some adsorption of fluoride onto the surfaces of both the AlCSS and the AlCMS sorbents occurred on adsorption sites with different energy levels according to the fit of data (high R^2 values between 0.85 and 0.9) for the Freundlich adsorption model. The K_L value for the AlCMS sorbent (0.333 L/mg) was smaller than the K_L value for the AlCSS sorbent (0.5 L/mg), and the 1/n value for the AlCMS sorbent (0.3153) was larger than the *1/n* value for the AlCSS sorbent (0.2432), while the E value for the AlCMS sorbent (2.09 kJ/mol) was smaller than the E value for the AlCSS sorbent (3.05 kJ/mol). According to the K_L values, the *1/n* values, and the E values determined for the adsorption of fluoride onto the AlCSS and AlCMS sorbents, the adsorption and binding of fluoride onto the surface of the AlCSS sorbent was stronger than the adsorption of fluoride onto the AlCMS sorbent.

The surface-normalized adsorption capacities of the AlCMS sorbent (952 μg/m^2) and the AlCSS sorbent (2273 μg/m^2) were determined by dividing the maximum adsorption capacity obtained from the Langmuir equation for each sorbent by the BET surface area of that sorbent. The results in Table 4 show that the surface-normalized adsorption capacity of the AlCSS sorbent was 2.4 times greater than the surface-normalized adsorption capacity of the AlCMS sorbent. While the surface area of the AlCSS sorbent was 1.22 orders of magnitude smaller than the surface area of the AlCMS sorbent, the surface-normalized adsorption capacity of the AlCSS sorbent was greater than that of the AlCMS sorbent. The greater observed surface-normalized adsorption capacity of the AlCSS sorbent despite its smaller surface area may be attributed to a greater distribution of aluminum on the surface of the AlCSS sorbent due to the higher percentage of aluminum present on the AlCSS sorbent surface, as shown in the SEM/EDX results.

Table 4. Comparison of surface-normalized adsorption capacities for the AlCSS and AlCMS sorbents based on Langmuir adsorption capacities.

Adsorbent	Adsorption Capacity (mg/kg)	BET Surface Area (m^2/g)	Surface-Normalized Adsorption Capacity (μg/m^2)
AlCSS sorbent	1430	0.6285	2273
AlCMS sorbent	10,000	10.5021	952

3.4. Effect of Adsorbent Surface Charge on Fluoride Adsorption

The results for the surface charge analysis of the AlCSS and AlCMS sorbents are presented in Figure 9. The results show that both the AlCSS and AlCMS sorbents exhibited a positive surface charge from pH 5 to pH 9 prior to attaining a pH_{PZC} of 9.6. Other aluminum-based adsorbents, such as α-Al_2O_3 and alum-impregnated activated alumina (AIAA), were shown to have similar pH_{PZC} values of 9.6 [43,44]. The addition of 5 mg/L fluoride to the background solution had a greater influence on the surface charge and behavior of the AlCSS sorbent, shifting the PZC to the left from pH 9.6 to pH 8.4, whereas the AlCMS sorbent's PZC shifted from pH 9.6 to pH 9.4. The major shift to the left of the PZC for the AlCSS sorbent indicates that the adsorption of fluoride onto the AlCSS sorbent occurred through inner-sphere complexation, which led to a markedly less positive surface of the AlCSS sorbent after the adsorption of the anionic fluoride species, resulting in the specific adsorption of fluoride onto the AlCSS sorbent surface. The smaller shift to the left of the PZC for the AlCMS sorbent indicates that the adsorption of fluoride onto the AlCMS surface occurred mostly through outer-sphere complexation, with some inner-sphere complexation occurring on the AlCMS sorbent surface. The stronger binding of fluoride observed for the AlCSS sorbent may be attributed in part to the greater specific adsorption of fluoride onto the AlCSS sorbent surface than the AlCMS sorbent surface.

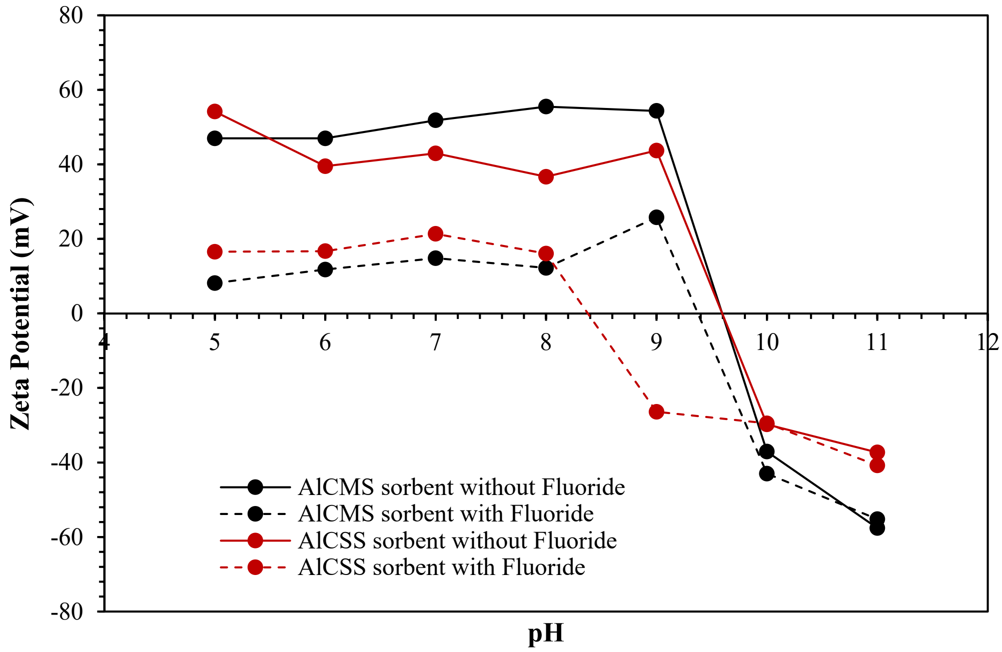

Figure 9. Zeta potential results for the AlCSS and AlCMS sorbents using 1 mM NaCl solution with and without 5 mg/L fluoride.

3.5. Effect of pH on Fluoride Adsorption

The effect of the initial solution on the adsorption and removal of fluoride is presented in Figure 10. The results from Figure 10 show that a greater-than-90-percent removal of fluoride occurred over a broad pH range from pH 3 to pH 10 for both the AlCSS and AlCMS sorbents, where the maximum removal of fluoride of about 98 percent was observed at pH 10 for both the AlCSS and AlCMS sorbents. Fluoride removal decreased as the pH increased from pH 10 to pH 11 for both the AlCSS and AlCMS sorbents. The removal of fluoride decreased approximately by 42% for the AlCSS sorbent, from 98% at pH 10 to 56% at pH 11, while the removal of fluoride decreased by about 32% for the AlCMS sorbent, from 98% at pH 10 to 65% at pH 11. These findings indicate that both the AlCSS and AlCMS sorbents would be applicable across a broad pH range from 3 to 10, which can be attributed to the pH_{PZC} value of 9.6 for both sorbents, due, mainly, to electrostatic attraction between the protonated surfaces of both sorbents and the negatively charged fluoride ions. Additionally, an excess of hydroxide ions (OH^-) alongside fluoride ions (F^-) can lead to competition for adsorption on the sorbent surface, even though the sorbent surface may still retain a positive charge [44].

The mechanisms affecting the adsorption of fluoride by the AlCSS and AlCMS sorbents may be described as follows:

$$(Al)OH_2^+ + F^- \leftrightarrow (Al)F + H_2O \tag{12}$$

$$(Al)\ OH + F^- \leftrightarrow (Al)F + OH^- \tag{13}$$

where the surfaces of both the AlCSS and AlCMS sorbents form protonated hydroxides of aluminum up to the pH_{PZC} of the adsorbents ($Al\text{-}OH_2{}^+$). At pH levels above 10, the formation of un-protonated hydroxide groups (Al-OH) on the surface of the sorbents resulted in a decrease in fluoride adsorption. The pH_{PZC} of both the AlCSS and AlCMS sorbents was 9.6, indicating that the surface of both adsorbents was protonated for the pH range from 3 to 9.6; therefore, the observed pH changes (lower final solution pH) for initial pH values from 3 to 10 were mainly due to the protonated acidic surface of both the AlCSS and AlCMS sorbents. The reaction producing hydroxide (Equation (13)) was applicable to the un-protonated surfaces of both the AlCSS and AlCMS sorbents for pH values greater than 9.6. As observed in Figure 10, the final pH of ~9 (AlCMS sorbent) and pH 10.7 (AlCSS sorbent) for an initial pH of 11 increased drastically due to the production of hydroxide (OH^-) versus the lower final pH values of pH 5.1 (AlCMS sorbent) and pH 6 (AlCSS sorbent) for an initial pH of 10. The results shown in Figure 10 indicate that the effect of pH on the adsorption of fluoride was similar for the protonated surfaces of both the AlCSS and AlCMS sorbents, while the effect of pH for the un-protonated surfaces was greater for the AlCSS sorbent that for the AlCMS sorbent. Based on the results from the surface charge analysis and the from the effect of pH on adsorption, the adsorption mechanism for the adsorption of fluoride onto both the AlCSS and the AlCMS sorbents was primarily due to electrostatic attraction between the positively charged surfaces of the two sorbents and the anionic fluoride species.

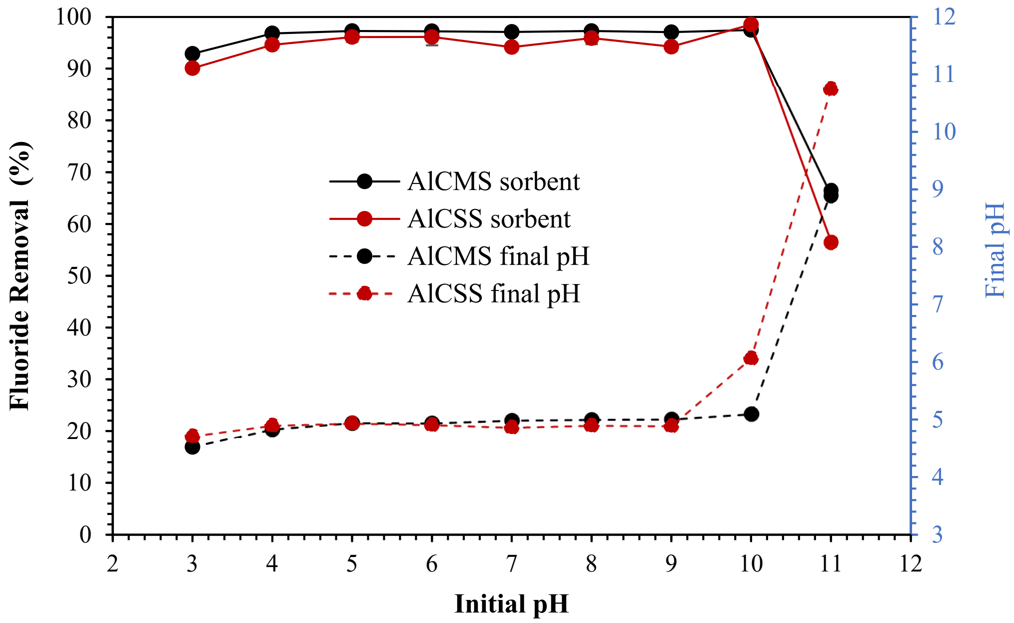

Figure 10. Effect of pH on the adsorption and removal of fluoride using 20 g/L dosage of AlCSS and AlCMS sorbents with a 5 mg/L initial fluoride concentration over 24 h.

3.6. Effect of Co-Existing Ions and Effect of Water Types on Fluoride Removal

Figure 11 shows the effect of co-existing ions on the removal of fluoride using the AlCSS and AlCMS sorbents. The results show that the removal of fluoride was not significantly affected in the presence of sulfate or calcium for both the AlCSS and AlCMS sorbents. The results show that the removal of fluoride in the presence of bicarbonate decreased appreciably for the AlCSS sorbent for bicarbonate concentrations from 1 mM to 5 mM, whereas the removal of fluoride in the presence of bicarbonate decreased significantly for the AlCMS sorbent only at a high bicarbonate concentration of 5 mM. This may be attributed to bicarbonate generating hydroxide ions, resulting in a competition with fluoride for the available surface adsorption sites [45]. A similar decrease in trend due to the presence of bicarbonate was observed with other metal-based sorbents [42,45–47].

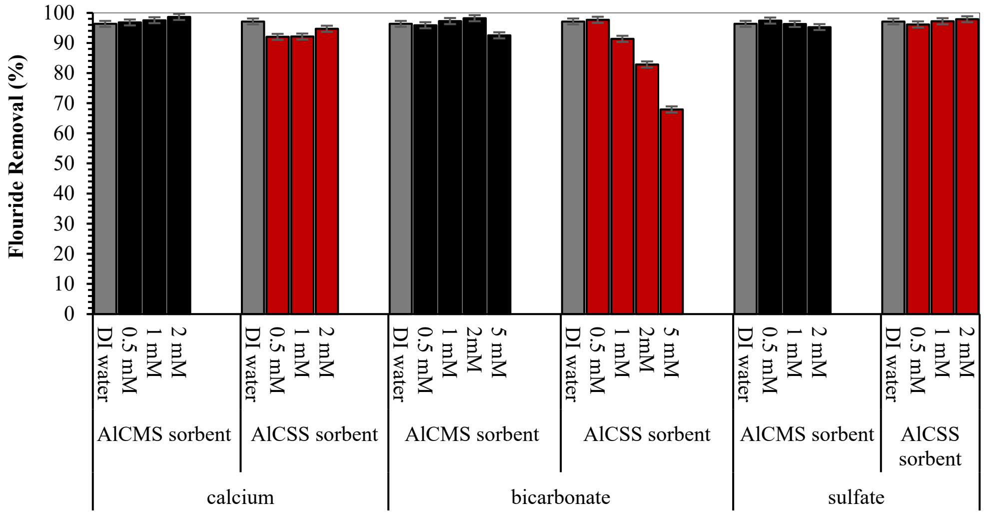

Figure 11. Effect of co-existing ions on the removal of fluoride using a 20 g/L dosage of the AlCSS and AlCMS sorbents with a 5 mg/L initial fluoride concentration over 24 h.

The results for the removal of fluoride from different water types are presented in Figure 12. The combined effect of the co-existing ions present in synthetic water (Table 1) on the removal of fluoride showed that, when the AlCMS sorbent was applied, it maintained its fluoride removal of nearly 98%, whereas fluoride removal decreased to 77% when the AlCSS sorbent was applied. When applied to tap water, ground water type 1 and groundwater type 2, the removal of fluoride using the AlCSS sorbent decreased to 82.6%, 82.2%, and 61.1%, respectively, whereas the removal of fluoride using the AlCMS sorbent remained at about 98% for all three types of water. The results presented in Figure 12 show that the AlCMS sorbent outperformed the AlCSS sorbent in terms of selectivity for the removal of fluoride from natural water sources, with appreciable levels of bicarbonate alkalinity, total hardness, and TDS.

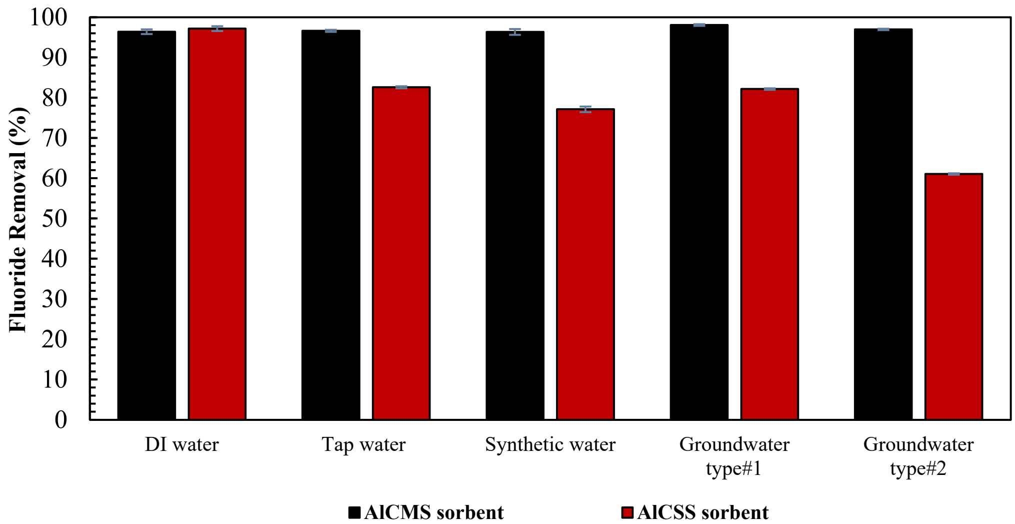

Figure 12. Effect of different water types on the removal of fluoride using 20 g/L of the AlCSS and AlCMS sorbents with a 5 mg/L initial fluoride concentration over 24 h.

3.7. Successive Adsorption Cycles' Study

Figure S4 shows the performance of the AlCSS and AlCMS sorbents for the removal of fluoride in the successive adsorption cycles' study using five consecutive 24 h adsorption cycles. The results show that the AlCMS sorbent was able to retain a fluoride removal performance greater than 90% for the first four consecutive adsorption cycles before decreasing to 63% for the fifth adsorption cycle. However, the AlCSS sorbent was able to retain its fluoride removal performance greater than 90% for only the first two consecutive adsorption cycles before decreasing to about 50% for the third adsorption cycle and to about 30% for the fourth and fifth adsorption cycles. The results from the successive adsorption cycles using five consecutive 24 h adsorption cycles showed that, after the second adsorption cycle, the fluoride removal performance of the AlCMS sorbent was better than the fluoride removal performance of the AlCSS sorbent. For the AlCSS sorbent, fewer fluoride adsorption sites were available on the surface of the AlCSS sorbent after two successive adsorption cycles, which resulted in the decreasing removal of fluoride after the second adsorption cycle. For the AlCMS sorbent, fewer fluoride adsorption sites were available on the surface of the AlCMS sorbent after four successive adsorption cycles, which resulted in the decreasing removal of fluoride after the fourth adsorption cycle.

4. Conclusions

This study compared the performance characteristics of two different crystalline silica base adsorbents coated with aluminum for the removal of fluoride from water: aluminum-coated silica sand (AlCSS) with a larger silica particle size and aluminum-coated microcrystalline silica (AlCMS) with a smaller silica particle size. Surface characterization of the two aluminum-coated adsorbents was carried out using XRD, TEM, and SEM/EDX, where the results showed that the aluminum coating for both the AlCSS sorbent and the AlCMS sorbent contained amorphous aluminum oxides. Fluoride adsorption by both the AlCSS sorbent and the AlCMS sorbent was found to be favorable according to the Langmuir and Freundlich adsorption equations. The adsorption capacity of the AlCMS sorbent was about seven times greater than the adsorption capacity of the AlCSS sorbent, while the adsorption of fluoride onto the AlCSS sorbent was stronger than adsorption of fluoride onto the AlCMS sorbent. The surface-normalized adsorption capacity of the AlCSS sorbent was found to be 2.4 greater than the surface-normalized adsorption capacity of the AlCMS sorbent. The rapid removal of fluoride within an hour was observed for both adsorbents, which followed second-order fluoride adsorption kinetics. The removal of fluoride occurred over a broad pH range from pH 3 to pH 10 for both the AlCSS and AlCMS sorbents, while both adsorbents had similar pH_{PZC} of about 9.6. The removal of fluoride by both adsorbents was not affected in the presence of calcium or sulfate, while the removal of fluoride was affected at higher concentrations of bicarbonate, with a larger decrease in fluoride removal observed for the AlCSS sorbent. The AlCMS sorbent displayed a higher fluoride selectivity for the removal of fluoride from several natural water sources.

Supplementary Materials: The following supporting information can be downloaded at https://www.mdpi.com/article/10.3390/separations11040125/s1: Figure S1: XRD patterns of (a) microcrystalline silica and (b) silica sand; Figure S2: (a) Pseudo-first-order kinetics plot for fluoride adsorption by AlCSS and AlCMS sorbents using an initial fluoride concentration of 5 mg/L and an adsorbent dosage of 20 g/L; (b) Pseudo-second-order kinetics plot for fluoride adsorption by AlCSS and AlCMS sorbents using an initial fluoride concentration of 5 mg/L and an adsorbent dosage of 20 g/L; Figure S3: (a) Intraparticle diffusion plot for AlCSS sorbent, and (b) intraparticle diffusion plot for AlCMS sorbent; and Figure S4: Successive adsorption cycles' study using 20 g/L of AlCSS and AlCMS sorbents with 5 mg/L initial fluoride concentration for 24 h adsorption cycles.

Author Contributions: K.M. and A.P.K. contributed to this study's conception and design. Material preparation, data collection, and analysis were performed by K.M. and J.W. The first draft of the manuscript was written by K.M., while the final manuscript was edited by A.P.K. All authors have read and agreed to the published version of the manuscript.

Funding: This work was supported by the University of Illinois, Chicago.

Data Availability Statement: The data presented in this study are available upon request from the corresponding author.

Acknowledgments: This study was conducted in the Department of Civil, Materials, and Environmental Engineering at the University of Illinois, Chicago.

Conflicts of Interest: The authors declare no conflicts of interest.

References

1. Nur, T.; Loganathan, P.; Nguyen, T.C.; Vigneswaran, S.; Singh, G.; Kandasamy, J. Batch and column adsorption and of fluoride using hydrous ferric oxide: Solution chemistry and modeling. *Chem. Eng. J.* **2014**, *247*, 93–102. [CrossRef]
2. Ali, S.; Thakur, S.K.; Sarkar, A.; Shekhar, S. Worldwide contamination of water by fluoride. *Environ. Chem. Lett.* **2016**, *14*, 291–315. [CrossRef]
3. Bhatnagar, A.; Kumar, E.; Sillanpää, M. Fluoride removal from water by adsorption-A review. *Chem. Eng. J.* **2011**, *171*, 811–840. [CrossRef]
4. Chen, A. *Design Manual: Removal of Fluoride from Drinking Water Supplies by Activated Alumina*; U.S. EPA Office of Research and Development: Washington, DC, USA, 2014; EPA/600/R-14/236.
5. UNESCO World Water Assessment Program. *The United Nations World Water Development Report 2021: Valuing Water*; UNESCO: Paris, France, 2021; pp. 1–187. Available online: https://unesdoc.unesco.org/notice?id=p::usmarcdef_0000375724 (accessed on 9 October 2023).
6. United Nations Educational, Scientific and Cultural Organization. *The United Nations World Water Development Report 2015*; UNESCO: Paris, France, 2015. [CrossRef]
7. WHO (World Health Organization). *Guidelines for Drinking—Water Quality*, 4th ed.; World Health Organization: Geneva, Switzerland, 2011; Volume 1.
8. Lacson, C.F.Z.; Lu, M.C.; Huang, Y.H. Chemical precipitation at extreme fluoride concentration and potential recovery of CaF2 particles by fluidized-bed homogenous crystallization process. *Chem. Eng. J.* **2021**, *415*, 128917. [CrossRef]
9. Ndiaye, P.I.; Moulin, P.; Dominguez, L.; Millet, J.C.; Charbit, F. Removal of fluoride from electronic industrial effluent by RO membrane separation. *Desalination* **2005**, *173*, 25–32. [CrossRef]
10. Tahaikt, M.; El Habbani, R.; Ait Haddou, A.; Achary, I.; Amor, Z.; Taky, M.; Alami, A.; Boughriba, A.; Hafsi, M.; Elmidaoui, A. Fluoride removal from groundwater by nanofiltration. *Desalination* **2007**, *212*, 46–53. [CrossRef]
11. Vaaramaa, K.; Lehto, J. Removal of metals and anions from drinking water by ion exchange. *Desalination* **2003**, *155*, 157–170. [CrossRef]
12. Lahnid, S.; Tahaikt, M.; Elaroui, K.; Idrissi, I.; Hafsi, M.; Laazit, I.; Amor, Z.; Tigal, F.; Elmidaoui, A. Economic evaluation of fluoride removal by electrodialysis. *Desalination* **2008**, *230*, 213–219. [CrossRef]
13. Vasudevan, S.; Kannan, B.S.; Lakshmi, J.; Mohanraj, S.; Sozhan, G. Effects of alternating and direct current in electrocoagulation process on the removal of fluoride from water. *J. Chem. Technol. Biotechnol.* **2011**, *86*, 428–436. [CrossRef]
14. Srimurali, M.; Pragathi, A.; Karthikeyan, J. A study on removal of fluorides from drinking water by adsorption onto low-cost materials. *Environ. Pollut.* **1998**, *99*, 285–289. [CrossRef]
15. Wan, K.; Huang, L.; Yan, J.; Ma, B.; Huang, X.; Luo, Z.; Zhang, H.; Xiao, T. Removal of fluoride from industrial wastewater by using different adsorbents: A review. *Sci. Total Environ.* **2021**, *773*, 145535. [CrossRef] [PubMed]
16. Damtie, M.M.; Woo, Y.C.; Kim, B.; Hailemariam, R.H.; Park, K.D.; Shon, H.K.; Park, C.; Choi, J.S. Removal of fluoride in membrane-based water and wastewater treatment technologies: Performance review. *J. Environ. Manag.* **2019**, *251*, 109524. [CrossRef] [PubMed]
17. He, J.; Yang, Y.; Wu, Z.; Xie, C.; Zhang, K.; Kong, L.; Liu, J. Review of fluoride removal from water environment by adsorption. *J. Environ. Chem. Eng.* **2020**, *8*, 104516. [CrossRef]
18. Inglezakis, V.J. The concept of "capacity" in zeolite ion-exchange systems. *J. Colloid Interface Sci.* **2005**, *281*, 68–79. [CrossRef] [PubMed]
19. Yadav, K.K.; Gupta, N.; Kumar, V.; Khan, S.A.; Kumar, A. A review of emerging adsorbents and current demand for defluoridation of water: Bright future in water sustainability. *Environ. Int.* **2018**, *111*, 80–108. [CrossRef] [PubMed]
20. Alhassan, S.I.; Huang, L.; He, Y.; Yan, L.; Wu, B.; Wang, H. Fluoride removal from water using alumina and aluminum-based composites: A comprehensive review of progress. *Crit. Rev. Environ. Sci. Technol.* **2021**, *51*, 2051–2085. [CrossRef]
21. Habuda-Stanić, M.; Ravančić, M.; Flanagan, A. A review on adsorption of fluoride from aqueous solution. *Materials* **2014**, *7*, 6317–6366. [CrossRef] [PubMed]
22. Kumari, S.V.A.; Sengupta, S. Adsorptive mitigation of fluoride ions using aluminosilicate adsorbents: A state-of-the-art review. *Environ. Chall.* **2021**, *5*, 100329. [CrossRef]
23. Cherukumilli, A.K. Designing a Scalable and Affordable Fluoride Removal (SAFR) Process for Groundwater Remediation in India. UC Berkeley. ProQuest ID: Cherukumilli_berkeley_0028E_17109. Merritt ID: Ark:/13030/m52v7nws. 2017. Available online: https://escholarship.org/uc/item/82t883n5 (accessed on 9 October 2023).
24. Modaresahmadi, K.; Khodadoust, A.P.; Wescott, J. Adsorption of fluoride from water using aluminum coated sand: Kinetics, equilibrium, effect of pH, and coexisting ions. *J. Geosci. Environ. Prot.* **2022**, *10*, 224–241. [CrossRef]
25. Ku, Y.; Chiou, H.-M. The adsorption of fluoride ion from aqueous solution by activated alumina. *Water Air Soil Pollut.* **2002**, *133*, 349–361. [CrossRef]

26. Salifu, A.; Petrusevski, B.; Ghebremichael, K.L.; Modestus, L.; Buamah, R.; Aubry, C.; Amy, G.L. Aluminum (hydr)oxide coated pumice for fluoride removal from drinking water: Synthesis, equilibrium, kinetics and mechanism. *Chem. Eng. J.* **2013**, *228*, 63–74. [CrossRef]
27. Ghorai, S.; Pant, K.K. Investigations on the column performance of fluoride adsorption by activated alumina in a fixed-bed. *Chem. Eng. J.* **2004**, *98*, 165–173. [CrossRef]
28. Ma, W.; Zhao, N.; Yang, G.; Tian, L.; Wang, R. Removal of fluoride ions from aqueous solution by the calcination product of Mg-Al-Fe hydrotalcite-like compound. *Desalination* **2011**, *268*, 20–26. [CrossRef]
29. Modaresahmadi, K.; Khodadoust, A.P.; Wescott, J. Adsorption of fluoride from water using Al–Mg–Ca ternary metal oxide-coated sand. *Water Supply* **2023**, *23*, 4699–4713. [CrossRef]
30. Gao, M.; Wang, W.; Cao, M.; Yang, H.; Li, Y. Hierarchical hollow manganese-magnesium-aluminum ternary metal oxide for fluoride elimination. *Environ. Res.* **2020**, *188*, 109735. [CrossRef] [PubMed]
31. Gao, M.; Wang, W.; Yang, H.; Ye, B.C. Efficient removal of fluoride from aqueous solutions using 3D flower-like hierarchical zinc magnesium-aluminum ternary oxide microspheres. *Chem. Eng. J.* **2020**, *380*, 122459. [CrossRef]
32. Chi, Y.; Chen, Y.; Hu, C.; Wang, Y.; Liu, C. Preparation of Mg-Al-Ce triple-metal composites for fluoride removal from aqueous solutions. *J. Mol. Liq.* **2017**, *242*, 416–422. [CrossRef]
33. Wang, M.; Yu, X.; Yang, C.; Yang, X.; Lin, M.; Guan, L.; Ge, M. Removal of fluoride from aqueous solution by Mg-Al-Zr triple-metal composite. *Chem. Eng. J.* **2017**, *322*, 246–253. [CrossRef]
34. Rice, E.W.; Baird, R.B.; Eaton, A.D. (Eds.) *Standard Methods for the Examination of Water and Wastewater*, 23rd ed.; American Public Health Association: Washington, DC, USA; American Water Works Association: Denver, CO, USA; Water Environment Federation: Alexandria, VA, USA, 2018; Method 4500-F-Fluoride.
35. Langmuir, I. The constitution and fundamental properties of solids and liquids. Part I. solids. *J. Am. Chem. Soc.* **1916**, *38*, 2221–2295. [CrossRef]
36. Freundlich, H. Über die Adsorption in Lösungen. *Z. Für. Phys. Chem.* **1907**, *57*, 385–470. [CrossRef]
37. Dubinin, M.M.; Radushkevich, L.V. Equation of the characteristic curve of activated charcoal. *Proc. Acad. Sci. USSR Phys. Chem. Sect.* **1947**, *55*, 331–333.
38. Lagergren, S. Zur Theorie der Sogenannten Adsorption Gelöster Stoffe. *Zeitschr. Chem. Ind. Kolloide* **1898**, *24*, 1–39.
39. Ho, Y.S.; McKay, G. Pseudo-second order model for sorption processes. *Process Biochem.* **1999**, *34*, 451–465. [CrossRef]
40. Weber, W.J.; Morris, J.C. Kinetics of adsorption on carbon from solutions. *J. Sanit. Eng. Div.* **1963**, *89*, 31–60. [CrossRef]
41. Maliyekkal, S.M.; Sharma, A.K.; Philip, L. Manganese-oxide-coated alumina: A promising sorbent for defluoridation of water. *Water Res.* **2006**, *40*, 3497–3506. [CrossRef]
42. Maliyekkal, S.M.; Shukla, S.; Philip, L.; Nambi, I.M. Enhanced fluoride removal from drinking water by magnesia-amended activated alumina granules. *Chem. Eng. J.* **2008**, *140*, 183–192. [CrossRef]
43. López Valdivieso, A.; Reyes Bahena, J.L.; Song, S.; Herrera Urbina, R. Temperature effect on the zeta potential and fluoride adsorption at the α-Al_2O_3/aqueous solution interface. *J. Colloid Interface Sci.* **2006**, *298*, 1–5. [CrossRef]
44. Tripathy, S.S.; Bersillon, J.L.; Gopal, K. Removal of fluoride from drinking water by adsorption onto alum-impregnated activated alumina. *Sep. Purif. Technol.* **2006**, *50*, 310–317. [CrossRef]
45. Amalraj, A.; Pius, A. Removal of fluoride from drinking water using aluminum hydroxide coated activated carbon prepared from bark of *Morinda tinctoria*. *Appl. Water Sci.* **2017**, *7*, 2653–2665. [CrossRef]
46. Kamble, S.P.; Deshpande, G.; Barve, P.P.; Rayalu, S.; Labhsetwar, N.K.; Malyshew, A.; Kulkarni, B.D. Adsorption of fluoride from aqueous solution by alumina of alkoxide nature: Batch and continuous operation. *Desalination* **2010**, *264*, 15–23. [CrossRef]
47. Biswas, K.; Gupta, K.; Ghosh, U.C. Adsorption of fluoride by hydrous iron(III)-tin(IV) bimetal mixed oxide from the aqueous solutions. *Chem. Eng. J.* **2009**, *149*, 196–206. [CrossRef]